Analytica Chimica Acta 1127 (2020) 131–139

Contents lists available at ScienceDirect

Analytica Chimica Acta

journal homepage: www.elsevier.com/locate/aca

Promotion effect of Zn on 2D bimetallic NiZn metal organic framework nanosheets for tyrosinase immobilization and ultrasensitive detection of phenol

Yangyang Wen [a, b], Rui Li [a], Jiahao Liu [a], Xin Zhang [a], Ping Wang [a], Xiang Zhang [a], Bin Zhou [a], Hongyan Li [b, *], Jing Wang [b, **], Zhenxing Li [a, ***], Baoguo Sun [b]

[a] College of New Energy and Materials, China University of Petroleum (Beijing), Beijing, 102249, China
[b] Beijing Advanced Innovation Center for Food Nutrition and Human Health, Beijing Technology and Business University (BTBU), 11 Fucheng Road, Beijing, 100048, China

HIGHLIGHTS

- 2D bimetallic NiZn-MOF NSs with tunable Ni/Zn ratios were synthesized.
- NiZn-MOF NSs were for the first time utilized to construct a tyrosinase biosensor.
- The fabricated biosensor exhibited a high sensitivity and an ultralow phenol detection limit.
- Zn element significantly enhanced the enzyme immobilization and biosensing activity of the bimetallic MOFs.

GRAPHICAL ABSTRACT

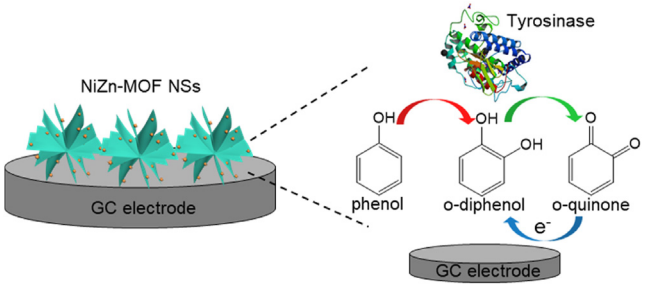

ARTICLE INFO

Article history:
Received 3 February 2020
Received in revised form
11 June 2020
Accepted 25 June 2020
Available online 11 July 2020

Keywords:
Metal organic frameworks
Nanosheets
Tyrosinase
Phenol detection
Biosensors

ABSTRACT

Environmental monitoring of pollutants is essential to guarantee the human health and maintain the ecosystem. The exploration of both simple and sensitive detection method has aroused widespread attentions. Herein, 2D bimetallic metal organic framework nanosheets (NiZn-MOF NSs) with tunable Ni/Zn ratios were synthesized, and for the first time employed to construct a tyrosinase biosensor. It is revealed that Zn element not only tuned the porosity structure and electronic structure of MOF NSs, but also modified their electrochemical activity. As a result, enzyme immobilization and electrochemical sensing performance of the NiZn-MOF NSs based biosensor were significantly enhanced by a suitable Zn addition. The fabricated tyrosinase biosensor exhibited excellent analytical detections, with a wide linear range from 0.08 μM to 58.2 μM, a high sensitivity of 159.3 mA M^{-1}, and an ultralow detection limit of 6.5 nM. In addition, the proposed biosensing approach also demonstrated good repeatability, superior selectivity, long-term stability, and high recovery for phenol detection in the real tap water samples.

1. Introduction

Phenol is an important reagent that has been widely used for production of various chemicals, including plastics, pharmaceuticals, petrochemicals, pesticides, and so on [1,2]. However, phenol

* Corresponding author.
** Corresponding author.
*** Corresponding author.
E-mail addresses: hongyan.li@btbu.edu.cn (H. Li), wangjing@th.btbu.edu.cn (J. Wang), lizx@cup.edu.cn (Z. Li).

https://doi.org/10.1016/j.aca.2020.06.062
0003-2670/

that released from chemical plants or landfill leachate pollutes the ground and surface water. Phenol has been marked as a dangerous material towards both nature and living organisms, since even a trace amount of phenol could cause muscular retardation, dizziness, vomiting, or liver and kidney damage [3]. The US Environment Protection Agency (EPA) and the European Union (EU) assigned the maximum amount of phenol compounds in fresh water as 0.5 μg L^{-1} and 0.1 μg L^{-1}, respectively [4]. For this reason, the rapid and accurate detection of phenol in water is significantly crucial for the sustainable management of water resources in the whole society.

Traditional analytical methods, such as high performance liquid chromatography-fluorescence detector [5,6], liquid chromatography mass-spectrometry [7], and gas chromatography-mass spectrometry [8], have been adopted for the detection of phenol compounds. However, these methods require experienced technicians, time-consuming sample preparations or expensive equipment, largely hindering their applications in emergent detections and on-site monitoring. In this connection, electrochemical biosensors are more advantageous for their low cost, fast response, and simplified operation [9]. With the aid of tyrosinase (Tyr, enzyme), phenol can be oxidized into quinone species and then reduced on the electrodes, generating characteristic electrochemical signals for the biosensor detection [10]. When constructing a electrochemical biosensor, electrode materials are essential to amply the electrochemical signals and enhance the detection performance [11]. Hence, various nanomaterials (such as graphene [12], carbon nanotubes [13] and noble metal particles [14]) have been explored, with good electrocatalytic activity, particle homogeneity, binding affinity with electrodes, and biocompatibility. However, their inadequate anchoring sites or low detection sensitivity significantly impede practical applications for these biosensors.

Metal-organic frameworks (MOFs) are a rising class of porous nanomaterials constructed by metal ions/clusters and organic linkers, and have shown their promising applications in the gas sorption and separation, catalysis, energy storage, chemical sensors, cancer therapy, and drug delivery [15–17]. Notably, owing to their large specific surface area, multiple chemical functionality, adjustable pore size, and strong affinity toward biomolecules, MOFs-based biosensors have been widely explored for the detection of various analytes [18]; plus, apparent interactions, including π-π stacking, hydrogen bonding, and electrostatic force, can be formed between the functional groups (-NH_2 or −COOH) in MOFs linkers and probe biomolecules, making MOFs excellent platforms for biomolecules and drug delivery systems in the environment or medicine applications. Up to date, a wide range of MOFs have been applied in the electrochemical biosensors, mainly focusing on the zeolitic imidazolate frameworks [19] (ZIF-70, ZIF-7, ZIF-8, ZIF-67, ZIF-68), MIL series (MIL-53 [20], MIL-100 [21], MIL-101 [22]), UiO series (UiO-66 [23]), BDC MOFs [9] and so on. Nevertheless, their biosensing applications are largely limited by their inherent drawbacks, including unsatisfactory catalytic activity and unsteadiness in water environments [24].

Recently, bimetallic MOFs have been widely studied in the electrochemical biosensors and shown promising catalytic activity. For example, Guo et al. prepared a CoMn-based MOFs/carbon nanofibers composite for detection of α-synuclein oligomers, which exhibited an excellent electrochemical activity and selectivity due to the synergistic effect of Co and Mn elements [25]; Wang et al. constructed a Tb-MOF-on-Fe-MOF conjugate as the platform for ultrasensitive detection of carbohydrate antigen 125, presenting an ultralow detection limitation and a high selectivity for the target analytes [26]; Gu et al. fabricated a bimetallic ZrHf-MOFs/carbon dots composite, which displayed remarkable sensing performance towards HER-2 cells [27]. It is revealed that the combination of diverse metal elements can introduce additional functionalities, while the synergistic effect of different metals improves the biocatalytic activity of MOFs. However, the rational design of bimetallic MOFs for electrochemical biosensors is still in its infancy, and more significantly, few bimetallic MOFs have been adopted to detect the phenol compounds.

In particularly, Ni-based MOFs usually show high stability, catalytic activity, low toxicity and good biocompatibility when used in the electrochemical biosensors [28]. Previous work also reported that Ni ions are conducive to adsorb strongly with the amino group in the enzymes, benefiting for the immobilization and steadiness of enzyme on the electrodes [29]. On the other hand, Zn ions is a nontoxic, highly stable and biocompatible element in the MOFs materials, which has been widely used as a heterometal to modify the morphology and catalytic activity in the alloys [30] or MOFs [16,31]. Therefore, in this work, the novel bimetallic NiZn-based MOF NSs were prepared and, for the first time, utilized to construct a tyrosinase biosensor. By constructing a two-dimensional (2D) nanostructure, the 2D MOF nanosheets could render a fast mass transport and charge transfer, as well as sufficient active sites accessible to catalytic reactions; by tuning the Ni/Zn ratios in the bimetallic MOFs, the promoted effect of Zn elements on the porosity structure, electronic structure, enzyme immobilization and phenol detection was revealed and optimized. More importantly, the fabricated biosensor exhibited remarkable detection performance, indicating that the obtained NiZn-MOF NSs can be a novel robust and versatile platform with a wide potential application in biomedical detection and environmental analysis.

2. Experimental section

2.1. Reagents

Chitosan (Chi, from shrimp shells, ≥ 75% deacetylated), tyrosinase (Tyr, from mushroom, lyophilized powder, > 1000 units·mg^{-1}), phenol, potassium hexacyanoferrate (III) and potassium hexacyanoferrate (II) trihydrate were purchased from Sigma-Aldrich (USA). Nickel(II) acetate tetrahydrate ($Ni(OAc)_2 \cdot 4H_2O$), zinc(II) sulfate heptahydrate ($ZnSO_4 \cdot 7H_2O$), *N*,*N*-dimethylacetamide (DMAC), terephthalic acid (1,4-H_2BDC), etc. were purchased from Energy Chemical Co., Ltd. (Shanghai, China). 50 mM phosphate buffer solution (PBS, pH = 6.0) was prepared by mixing standard solutions of Na_2HPO_4 and NaH_2PO_4. Milli-Q water (18 MΩ cm) was used throughout all electrochemical experiments.

2.2. Apparatus

The scanning electron microscopy (SEM) and energy dispersive X-ray spectroscopy (EDS) were taken with a Hitachi SU8010. Transmission electron microscopy (TEM) was performed on a JEM 2100 LaB6. Powder X-ray diffraction (XRD) patterns were obtained on a Bruker D8 Advance instrument with a Cu Kα irradiation source at a scanning rate of 1° per min. X-ray photoelectron spectroscopy (XPS) was collected on a PHI5000 Versaprobe using an Al Kα X-ray source, with the binding energies calibrated to C 1s peak at 285.0 eV. The specific surface areas and pore size distribution of samples were evaluated on the ASAP2460 Surface Area and Porosity Analyzer (Micromeritics), calculated by N_2 sorption isotherms using a Brunauer-Emmett-Teller (BET) method.

All electrochemical measurements were performed on a CHI660D electrochemical workstation (Shanghai CH Instrument, China) using a standard three-electrode system. A modified glassy carbon (GC, 3 mm in diameter) electrode was used as the working electrode, an Ag/AgCl electrode as the reference electrode, and a

platinum foil as the counter electrode. Electrochemical impedance spectroscopy (EIS) was studied in 1 mM $K_3[Fe(CN)_6]/K_4[Fe(CN)_6]$ (1:1) containing 0.5 M KNO_3 on a Metrohm Autolab PGSTAT 302 N Potentioatat/Galvanostat (Eco Chemie, Netherlands) with a frequency range from 0.1 Hz to 10 kHz.

2.3. Preparation of bimetallic NiZn-MOF NSs

To prepare the bimetallic NiZn-MOF NSs, 0.1 mmol $Ni(OAc)_2 \cdot 4H_2O$ and 0.03 mmol $ZnSO_4 \cdot 7H_2O$ were first dissolved in 6 mL water. Then, 6 mL DMAC solution containing 0.05 mmol of 1,4-benzenedicarboxylic acid (1,4-H_2BDC) was added into the above solution and stirred for 30 min. The well-mixed solution was then transferred to a Teflon-lined stainless-steel container (20 mL) and heated at 150 °C for 3 h. The obtained product, assigned to NiZn-MOF NSs, was collected by centrifugation, washed with ethanol and water, and dried at 60 °C for 12 h. For comparison, another two NiZn-MOF products were also synthesized using the same method but with different amounts of $ZnSO_4 \cdot 7H_2O$ (0.01 mmol and 0.05 mmol), designated as NiZn-MOF-1/3 and NiZn-MOF-5/3, respectively. Plus, the monometallic Ni-MOF and Zn-MOF were also prepared. A similar experimental procedure was adopted without the addition of $ZnSO_4 \cdot 7H_2O$ to prepare the Ni-MOF and without the addition of $Ni(OAc)_2 \cdot 4H_2O$ for Zn-MOF.

2.4. Fabrication of tyrosinase biosensor

The tyrosinase biosensor was fabricated via a facile casting method. GC electrode was first polished with alumina powders (1.0, 0.3, and 0.05 μm, sequentially), washed with Milli-Q water and ethanol, and dried with purified nitrogen stream. Then, the tyrosinase biosensor was prepared as follows: 20 μL of catalyst suspension (NiZn-MOF, 0.8 mg mL^{-1}) was added to 10 μL of chitosan solution (Chi, 6 mg mL^{-1}, dissolved in 2% acetic acid aqueous solution and adjusted to pH 5.0 using 10% NaOH solution), followed by sonication for 20 min; 10 μL of tyrosinase solution (Tyr, 10 mg mL^{-1} in PBS) was added to the above solution and sonicated for 5 min. 5 μL of the above mixture was cast onto the newly polished GC electrode, producing a uniform Tyr-NiZn-MOF-Chi/GC electrode. For storage, the fabricated GC electrode was kept in a refrigerator at 4 °C. Before electrochemical measurements, the prepared enzyme electrode was immersed in 50 mM PBS (pH = 6.0) for 30 min to remove residual components. In the fabricated Tyr-NiZn-MOF-Chi/GC biosensor, chitosan was added to produce a good composite film and improve the stability of the biosensor, owing to its excellent film-forming ability, adhesion ability, non-toxicity and high mechanical strength properties [32]; The NiZn-MOF served as the matrix, facilitating enzyme immobilization owing to its high surface area and plentiful grafting groups (mainly −COOH on the surface [16]) to form chemical bindings or electrostatic adsorption with the enzymes.

2.5. Detection of phenol

Cyclic voltammetry (CV) measurements were conducted in pH 6.0 PBS solution at a scan rate of 100 mV s^{-1} ranging from +0.4 V to − 0.4 V. The amperometric current-time (I-t) curves for phenol were performed to investigate the detection performances of different electrodes. Under an applied potential value of − 0.05 V, the I-t curves were performed in 30 mL PBS stirring with successive addition of standard phenol solution at appropriate time intervals at room temperature. Real water samples were also detected by similar amperometric I-t tests.

3. Results and discussion

3.1. Characterization of bimetallic NiZn-MOF NSs

The bimetallic NiZn-MOF NSs were synthesized via a facile one-step solvothermal method, as illustrated in Scheme 1. During this solvothermal process, Ni^{2+}, Zn^{2+}, and 1,4-H_2BDC ligands were first nucleated, formed the NiZn-MOF nanosheets and then further assembled into the flower-like clusters. It is noting that the flower-like structure assembled from nanosheets renders open structure with high specific surface areas and fast electron/mass transfer channels, which is more favorable for high enzyme loadings and catalytic activities (will be discussed later); plus, the plentiful grafting groups, mainly −COOH, on the MOF ligands can easily form chemical bindings or electrostatic adsorption with the enzymes, significantly enhancing the enzyme immobilization [16].

The as-prepared NiZn-MOF NSs were first analyzed by powder X-ray diffraction (XRD) patterns, as shown in Fig. 1A. The main peaks are centered at 9.3°, 15.6°,18.3° and 19.1°, in good agreement with those of nickel hydroxide terephthalate hydrate phase (JCPDS No.035–1677) [16], indicating the successful synthesis of MOF material. The XRD patterns in Fig. S1 show that the monometallic Ni-MOF and NiZn-MOF share the similar XRD patterns, indicating that the introduction of Zn^{2+} does not affect the crystal structure of Ni-MOF. The morphology of NiZn-MOF NSs was then investigated by scanning electron microscopy (SEM) and transmission electron microscopy (TEM), revealing the flower-like cluster structure of NiZn-MOF NSs. The clusters are a few microns in size, consisting of ultrathin nanosheets assembled together, as shown in Fig. 1B–C. TEM image in Fig. 1D further confirms the flower-like structure of NiZn-MOF NSs and shows that the edges of these nanosheets tend to curl or blend, revealing their flexible nature.

The elemental composition of NiZn-MOF NSs was subsequently studied by energy dispersive X-ray spectroscopy (EDS, Table S1), indicating a molar ratio of Ni/Zn is calculated to be 1.74/1. Further, X-ray photo-electron spectroscopy (XPS) was also investigated, in which Ni, Zn, C, and O elements were clearly identified (Fig. S2A), confirming the synthesis of bimetallic MOF. Fig. S2B and S2C display the high-resolution Ni 2p and Zn 2p XPS spectra, with Ni $2p_{3/2}$ at 855.6 eV and Zn $2p_{3/2}$ at 1021.8 eV, respectively. It should be noted that all binding energies were calibrated to C 1s peak at 285.0 eV. Compared to the monometallic Ni-MOF, a clear shift to higher energy (0.3 eV) is observed for the Ni 2p peaks in the bimetallic NiZn-MOF NSs; whereas, a negatively shift is observed for the Zn 2p spectra, indicating the charge transfer between the metal ions and the surrounding atoms, causing Ni^{2+} more positively charged and Zn^{2+} less positively charged. It is speculated that the charge transfer may be resulted from the interaction or synergistic effect of these two metal ions. Similar phenomena were also reported in previous NiFe-LDH/MXene work [33] and noble metal supported CoO(OH), which could significantly prompt the catalytic activity of samples [34].

A series of NiZn-MOF were also studied by adopting a fixed Ni^{2+} amount (0.1 mmol) and varied Zn^{2+} amounts (0.01–0.05 mmol) in the precursors (see Experimental section). NiZn-MOFs withlower Zn^{2+} loadings (NiZn-MOF-1/3 and NiZn-MOF) present a similar nanosheet structure as the Ni-MOF (Fig. S3A-B, Fig. 1C), indicating the evenly incorporation of Zn^{2+} ions in the Ni-MOF crystal; however, the NiZn-MOF with higher Zn^{2+} loading (NiZn-MOF-5/3) shows a much thicker sheet structure (Fig. S3C), revealing that high concentration of Zn^{2+} increases the thickness of the nanosheets in MOF. To further analyze the porosity features of samples, nitrogen adsorption/desorption isotherms were carried out (Fig. S4). The MOF samples show type IV isotherms with obvious hysteresis loops at a range of 0.4–1.0 in the relative pressure, suggesting the

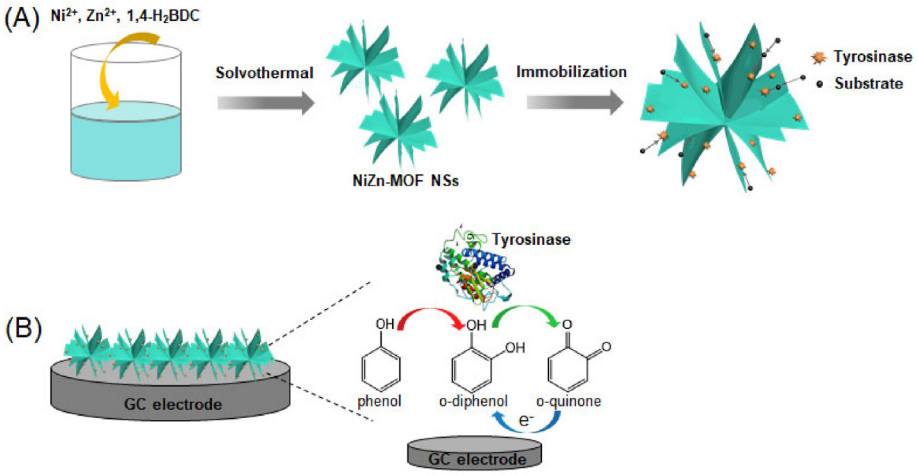

Scheme 1. (A) Schematic diagram of the synthetic procedure for NiZn-MOF NSs and the tyrosinase biosensor. (B) Electrochemical reactions occurred in the NiZn-MOF NSs modified GC electrode.

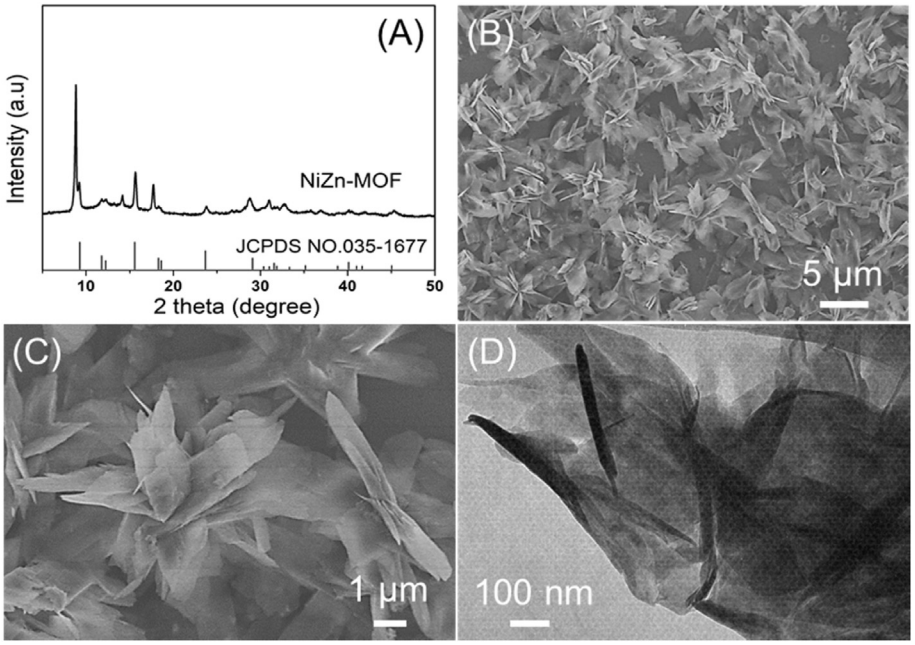

Fig. 1. (A) XRD patterns of NiZn-MOF NSs. Typical SEM (B–C) and TEM (D) images of NiZn-MOF NSs.

existence of mesopores in these materials [35,36]. The specific surface areas (S_{BET}) are as follows: 30.3 m^2 g^{-1} for Ni-MOF, 37.6 m^2 g^{-1} for NiZn-MOF-1/3, 40.1 m^2 g^{-1} for NiZn-MOF, 16.6 m^2 g^{-1} for NiZn-MOF-5/3, and 11.2 m^2 g^{-1} for Zn-MOF. These values indicate that the inclusion of Zn^{2+} slightly increased the S_{BET} of the MOFs, with NiZn-MOF sample having the largest value. The S_{BET} results are consistent with the morphologies of the MOF NSs (SEM characterizations in Fig. 1 and Fig. S3).

3.2. Electrochemical performance of NiZn-MOF NSs based biosensor

The electrochemical activity and electron transfer properties of as-constructed biosensor are largely affected by its conformation and structure. Therefore, cyclic voltammetry (CV) and electrochemical impedance spectroscopy (EIS) measurements were first conducted in 1 mM $Fe(CN)_6^{3-}/^{4-}$ solution (containing 0.5 M KNO_3), revealing the interfacial properties of the nanocatalyst-modified electrode. As shown in Fig. 2A, an apparent pair of redox peaks (0.1–0.35 V) are observed at the bare GC electrode, attributing to the fast redox reaction of $Fe(CN)_6^{3-}/^{4-}$ ions. However, the peak currents are significantly suppressed at the Tyr-Chi/GC electrode, mainly resulted from the formation of a thick Tyr-Chi film on the electrode and the blocked conductivity [37]. When adding NiZn-MOF NSs into the Tyr-Chi film, the current responses are significantly enhanced, indicating the high biocatalytic activity of NiZn-MOF nanocatalyst.

Fig. 2B displays the EIS plots of the electrodes, which can be divided into a semicircular part at the high frequency and a linear part at the low frequency. The linear part links to the diffusion process, and the semicircular part discloses the electron transfer process [38–40]. The diameter of the semicircular part equals to the electron transfer resistance, and reveals the blocking behavior of the redox couple at the modified electrode [41,42]. The plot of the bare GC electrode is nearly a straight line, indicating a diffusion-

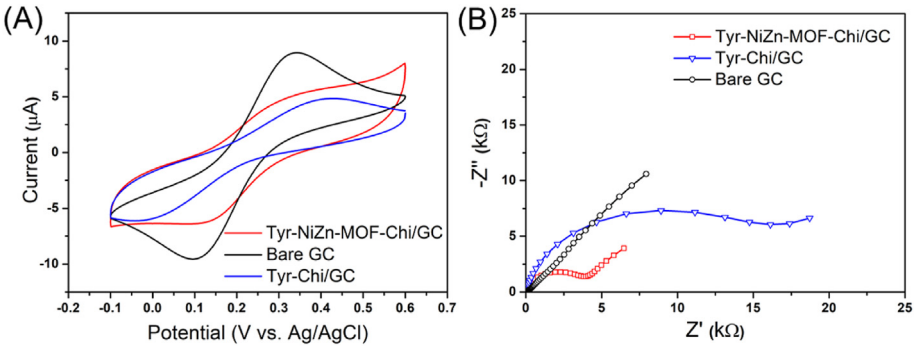

Fig. 2. (A) CV curves of different electrodes in 1 mM $Fe(CN)_6^{3-/4-}$ solution containing 0.5 M KNO_3 at a scan rate of 100 mV s^{-1}. (B) Nyquist plots of different electrodes in 1 mM $Fe(CN)_6^{3-/4-}$ containing 0.5 M KNO_3.

limited process and a fast electron transfer rate. The Tyr-Chi/GC electrode shows a large semicircle in the EIS plot, indicating a significantly impeded electron transfers between $Fe(CN)_6^{3-/4-}$ and the electrode surface due to the formation of a Tyr-Chi layer. Even though the chitosan could reduce the electron transfer rate on the electrode surface, it is still an indispensable component for enzyme biosensors when the good film-forming ability and a biocompatible microenvironment are required [43]. Nevertheless, after adding NiZn-MOF NSs into the Tyr-Chi layer, a much smaller semicircle of the plot is observed than that of the Tyr-Chi/GC electrode, revealing significantly improved electron transfer on the electrode by the modification of NiZn-MOF NSs.

The electrochemical activity of the Tyr-NiZn-MOF-Chi/GC electrode was then characterized by CV in the presence of phenol. Fig. S5A is the CV plots of the Tyr-NiZn-MOF-Chi/GC in N_2-saturated PBS aqueous solution at various scan rates. It is clear that the obtained cathodic and anodic peak currents increase linearly with the increase of scan rates from 40 to 200 mV s^{-1} (Fig. S5B), implying a surface-controlled electrochemical process and fast electron transfer between the enzyme and GC electrode [44]. Fig. 3 presents CV curves of the Tyr-NiZn-MOF-Chi/GC biosensor with and without the addition of phenol in air-saturated PBS solution. After adding phenolaqueous solution. After the addition of phenol, the redox currents increase obviously, suggesting that the tyrosinase catalyzed redox reaction occurred on the surface of electrode with a high biocatalytic activity for phenol substrate. Note that a large

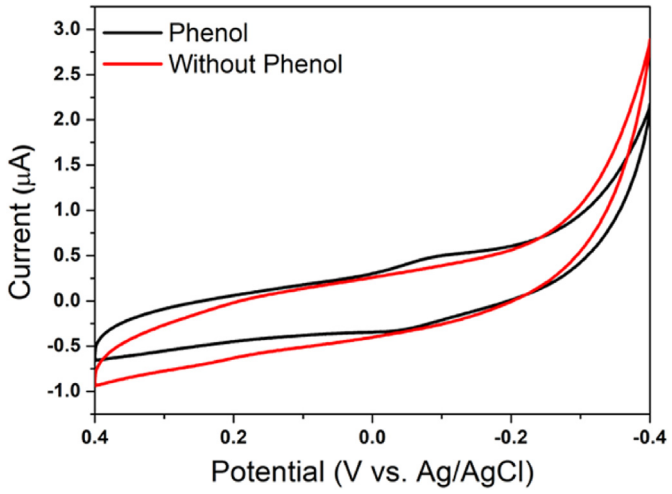

Fig. 3. CV curves of the Tyr-NiZn-MOF-Chi/GC biosensor with and without the addition of phenol (3 mM) in air-saturated 50 mM pH 6.0 PBS at 100 mV s^{-1}.

current response toward phenol was detected from the potential of −0.05 V vs. Ag/AgCl. To reduce background noises and obtain a low detection limit, we selected −0.05 V vs. Ag/AgCl as the detection potential for further amperometric measurements.

The current response of the electrochemical biosensors strongly relies on the experimental conditions, such as pH value, nanocatalyst loaded or enzyme mass [45]. For this reason, the effect of pH on the biosensor response was examined in the 10 μM phenol+50 mM PBS system (Fig. S6A). The maximum current response of the biosensor reaches at pH 6.0 and the current response decreases at pH > 6 or pH < 6 conditions. Thus, a neutral condition (pH 6.0) is selected in the further experiments to achieve a higher enzyme activity. Plus, biosensor responses towards the enzyme concentrations were also studied (Fig. S6B). The biosensor current increases as the tyrosinase concentration increases, achieving a maximum value at 10 mg mL^{-1}; whereas, the current decreases gradually with the tyrosinase concentration further increases. As we know, a low enzyme loading is insufficient to cover the surface of the electrode entirely, weakening the whole catalytic reaction; however, a large enzyme loading would increase the thickness of the composite film and impede electron transfer in the catalytic reaction. Fig. S6C discloses the effect of NiZn-MOF concentration on the biosensor response. When the concentration of NiZn-MOF nanocatalyts increase from 0.2 to 0.8 mg mL^{-1}, the current response is significantly enhanced; on the other hand, the current response of the biosensor decreases after the concentration of NiZn-MOF is beyond 0.8 mg mL^{-1}. It is speculated that the NiZn-MOF amount affects the porous structure in the composite film, which would change the electron transfer process and the biocatalytic activity of the biosensor, showing an optimized current response towards the NiZn-MOF amounts. In the composite film, chitosan was added to improve the film-forming ability of the biosensor and to facilitate the enzyme immobilization. According to Fig. S6D, the optimized concentration of chitosan in the composite film is 6 mg mL^{-1}. Lower chitosan amount is not benefit for the film formation; while larger amount increases the thickness of the film and hinders the electron transfer in the film. In sum, 10 mg mL^{-1} of tyrosinase, 0.8 mg mL^{-1} of NiZn-MOF and 6 mg mL^{-1} of chitosan were utilized in the subsequent experiments.

The detection mechanism of the nanocatalyst-based tyrosinase biosensor has been reported in previous works [32,46,47]. With the presence of oxygen and tyrosinase, phenol is first oxidized into the corresponding *o*-diphenol, which would be further oxidized into *o*-quinone. Then, *o*-quinone is electrochemically reduced to *o*-diphenol on the electrode surface to cyclically amplify the electrochemical signals. Based on this mechanism, a detection mechanism of the NiZn-MOF based tyrosinase biosensor was plotted in Scheme 1B. It is worth noting that the ultrathin nanosheet

structure and the plentiful grafting groups (mainly −COOH [16]) of the NiZn-MOF are favorable for the enzyme immobilization, while the sufficient catalytic sites (metal ions) promote catalytic reactions, making NiZn-MOF an excellent platform for biosensors.

Fig. 4A shows the amperometric current-time responses of the Tyr-NiZn-MOF-Chi/GC and Tyr-Chi/GC biosensors at −0.05 V with the successive additions of phenol in PBS under constant stirring. Both electrodes present quick and clear current response with the increase of phenol concentrations. It is notable that the current response of Tyr-NiZn-MOF-Chi/GC electrode is significantly larger than that of Tyr-Chi/GC electrode, verifying that the NiZn-MOF NSs modified electrode processes much a high biocatalytic activity. The response time of Tyr-NiZn-MOF-Chi/GC is less than 5 s (achieving 94% of steady state current), indicating a fast mass transport and charge transfer process can be accomplished between the enzyme and phenol substrate. The open structure of NiZn-MOF could aid the diffusion of phenol on the tyrosinase surface, realizing a rapid bio-electrocatalytic reaction (see Scheme 1). The corresponding calibration curves of steady-state currents versus phenol concentrations were plotted in Fig. 4B. The currents linearly increase with the growing of phenol contents, with a wide linear range from 0.08 μM to 58.2 μM, and the responding sensitivity is 159.3 mA M^{-1}. These data are apparently much better than the previous metal particles [48], carbon nanotube [14] or graphene [12] modified tyrosinase electrodes, as listed in Table 1. The detection limit is another indicator for the biosensor properties. The estimated detection limit for NiZn-MOF NSs based biosensor is only 6.5 nM at a signal-to-noise ratio of 3, which is significantly much lower than the reported values (Table 1), demonstrating the remarkable detection performance of NiZn-MOF NSs in this work.

To better understand the catalytic mechanism of the bimetallic MOF nanocatalysts, the electrochemical activity of NiZn-MOF-1/3 (with less Zn^{2+} loading) and NiZn-MOF-5/3 (with more Zn^{2+} loading) were also conducted. As shown in Fig. 5 and Table S2, both electrodes show lower current responses and sensitivity (134.3 mA M^{-1} for NiZn-MOF-1/3; 92.9 mA M^{-1} for NiZn-MOF-5/3), compare to NiZn-MOF sample (159.3 mA M^{-1}), revealing an optimal Zn^{2+} loading to achieve the best electrochemical activity. Plus, the sensitivity of NiZn-MOF-1/3 modified electrode is significantly higher than the pristine Ni-MOF (90.2 mA M^{-1}), disclosing that the addition of Zn^{2+} could significantly improve the catalytic activity of MOF material. However, when introducing higher Zn^{2+} content (as illustrated in NiZn-MOF-5/3), the electrochemical activity would be reduced, with the lowest sensitivity in pure Zn-MOF (only 80.5 mA M^{-1}). These results demonstrated that Zn element plays a promoted effect on the electrochemical activity in the bimetallic MOF nanocatalyst.

Based on the results discussed above, we speculate that the best catalytic activity of the NiZn-MOF may be attributed to the following points: (1) Ultrathin nanosheet structure and the improved specific surface area. SEM observations demonstrated that NiZn-MOF remained the ultrathin nanosheet structure as the pristine Ni-MOF (Fig. 1 and Fig. S3) but exhibited a higher S_{BET} value than the other samples (Fig. S3), revealing the improved porosity structure after the inclusion of Zn^{2+}, which could enhance the enzyme immobilization (by forming chemical bindings or electrostatic adsorption with the plentiful grafting groups, mainly −COOH) [16]. (2) Synergistic effect of the two metal elements. The enhanced catalytic activity was reported in the bimetal alloys [54] or bimetallic MOF materials [55] based electrocatalytic reactions, mainly attributed to the synergistic effect of two metal elements and modified electronic structure by the strong interplay effect (see XPS results in Fig. S2). (3) Improved conductivity of the MOF electrodes. EIS plots of different MOF electrodes were measured, and the fitted equivalent circuit diagram was plotted (insert) in Fig. S7. The fitted data is listed in Table S3. The electron transfer resistance (R2) values are in the consequence: NiZn-MOF-1/3 (0.399 kΩ) < NiZn-MOF (0.408 kΩ) < Ni-MOF (1.000 kΩ) < NiZn-MOF-5/3 (1.200 kΩ) < Zn-MOF (1.840 kΩ). This data indicates that the lower Zn^{2+} loadings could significantly improve the electron transfers between the enzyme and the electrode, while NiZn-MOF with high Zn^{2+} loading and pristine Zn-MOF show much higher R2 values, further explaining their poor electrochemical biocatalytic performances.

3.3. Reproducibility, selectivity, stability and real sample application of the biosensor

The repeatability and reproducibility of biosensors are critical factors for real-life applications [37]. The repeatability of Tyr-NiZn-MOF-Chi/GC electrode was tested by continuously measuring their current response to 3 μM phenol. The current response of the biosensor was performed in 11 consecutive measurements, and the relative standard deviation (RSD) value for the electrodes is 2.23%, revealing the good repeatability of the fabricated biosensor. Similarly, three different electrodes were conducted to evaluate the electrode-to-electrode manufacturing reproducibility. The RSD value for the three individual biosensors is 1.84%, showing the excellent inter-electrode reproducibility.

Another important issue in the use of biosensors is their selectivity, that is, their anti-interference ability to other substances [56]. We used some common interfering substances to detect the distinction between phenol and target molecules. Fig. S8 shows when adding dropwise 3 μM phenol, there was a significant change in current, and when adding its 100 times concentration of K^+, Mg^{2+}, Ca^{2+}, Fe^{3+}, Zn^{2+}, SO_4^{2-}, PO_4^{3-}, CO_3^{2-}, NO_3^-, 10-fold excess of

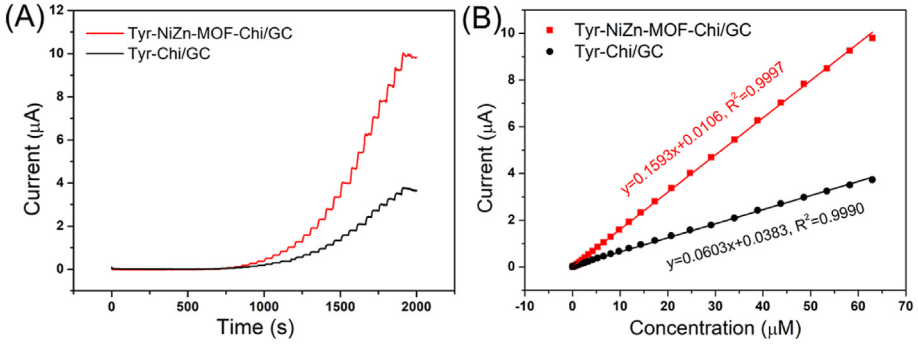

Fig. 4. (A) Amperometric I-t curves of the Tyr-NiZn-MOF-Chi/GC electrode with successive additions of phenol in a 50 mM PBS (pH = 6.0) at a potential of − 0.05 V versus Ag/AgCl. (B) The corresponding calibration curves of steady-state currents versus phenol concentrations.

Table 1
A comparison of the sensing performance in this work and previous works.

Modified electrode	Analyte	Linear range (μM)	Sensibility (mA·M^{-1})	Detection Limit (nM)	Reference
Tyr-NiZn-MOF/GCE	Phenol	0.08–58.2	159.3	6.5	This work
Tyr-GO-ZnO/GCE	Phenol	5–175	–	2.2	[49]
Tyr-MWNTs/GCE	Phenol	0.4–10	–	200	[50]
Tyr-Au-HA/GCE	Phenol	0.07–5	1.77	10	[48]
Tyr-CNTs/Au NPs	Phenol	0.01–0.2	131	2.94	[14]
Tyr-Graphene-Aminoac/GCE	Phenol	0.001–21	4.08	0.35	[12]
Tyr-EDS-NHS/GCE	Phenol	0.5–30	8	260	[51]
Tyr-Thionine/CPE	BPA	0.15–45	85.4	150	[52]
Tyr-CNTs/GCE	Phenol	1.0–19	303	130	[53]

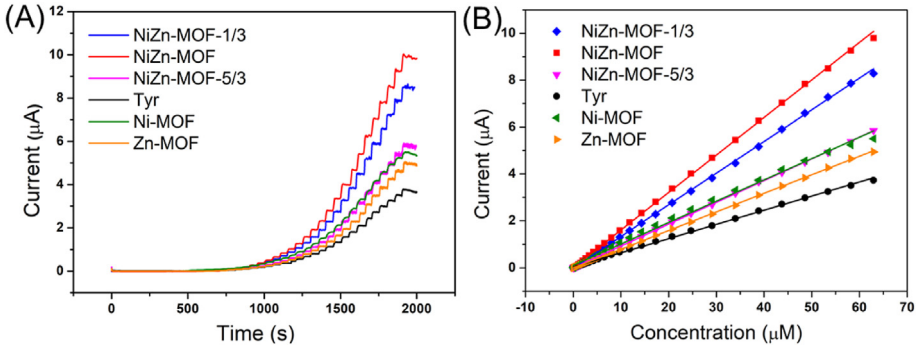

Fig. 5. (A) Amperometric I-t curves of the nanocatalyst-modified electrodes with successive additions of phenol in a 50 mM PBS (pH = 6.0) at − 0.05 V versus Ag/AgCl. (B) The corresponding calibration curves of steady-state currents versus phenol concentrations.

uric acid (UA) and ascorbic acid (AA), and 50-fold concentration of glucose (Glc), the current did not change significantly. When phenol was added again, the current changed significantly. Therefore, it shows that this biosensor has strong anti-interference ability and high selectivity.

The storage stability of the biosensor was also evaluated by measuring CV responses to the phenol substrate (3 μM). When the enzyme electrode was not in use, it was sealed and stored in a refrigerator at 4 °C. The results showed that the biosensor retained up to 93% of the original response after a five-week continuous test, demonstrating the long-term stability of the biosensor. To further verify the potential application of the fabricated biosensor in real water sample detection, the biosensor was applied to the standard addition method for the determination of phenol in actual water samples. The recovery test was studied by adding spiked phenol to tap water. Before use, the tap water sample was filtered through a 0.45 μm filter to remove suspended solids. The sample was evaluated by using amperometric method to observe the response of tap water spiked with 0.5 μM and 50 μM phenol. The recovery of the electrode was from 97.4% to 102.31% (Table S4), indicating that the developed biosensor has satisfactory accuracy and confirming the designed biosensor has the potential to detect phenol in real water samples.

4. Conclusions

In summary, 2D bimetallic NiZn-MOF NSs with tunable Ni/Zn ratio were synthesized, and for the first time utilized to fabricate a tyrosinase biosensor. The porosity structure, electronic structure, and electrochemical activity of NiZn-MOF NSs were modified by the addition of Zn contents, making NiZn-MOF NSs a remarkable immobilization platform for the tyrosinase. The fabricated biosensor exhibited excellent analytical performance over a wide linear range of 0.08–58.2 μM, with a high sensitivity of 159.3 mA M^{-1} and an ultralow detection limit of 6.5 nM. Plus, the obtained tyrosinase biosensor showed good reproducibility and stability. The remarkable bio-sensing performance is mainly attributed to the enhanced specific surface area, catalytic activity and conductivity due to the synergistic effect of the two metal elements. This work may pave a new insight into the development of novel electrode materials for the biomedical detection and environmental analysis using the electrochemical techniques.

CRediT authorship contribution statement

Yangyang Wen: Conceptualization, Methodology, Writing - original draft. **Rui Li:** Methodology, Investigation. **Jiahao Liu:** Investigation. **Xin Zhang:** Investigation. **Ping Wang:** Investigation. **Xiang Zhang:** Investigation. **Bin Zhou:** Investigation. **Hongyan Li:** Conceptualization, Methodology, Writing - original draft. **Jing Wang:** Conceptualization, Writing - review & editing. **Zhenxing Li:** Supervision, Writing - review & editing. **Baoguo Sun:** Writing - review & editing.

Declaration of competing interest

The authors declare that they have no known competing financial interests or personal relationships that could have appeared to influence the work reported in this paper.

Acknowledgments

This work was supported by National Natural Science Foundation of China (31901729) and School Level Cultivation Fund of Beijing Technology and Business University for Distinguished and Excellent Young Scholars (BTBUYP2020).

Appendix A. Supplementary data

Supplementary data to this article can be found online at https://doi.org/10.1016/j.aca.2020.06.062.

References

[1] R. Lu, W. Li, B. Mizaikoff, A. Katzir, Y. Raichlin, G. Sheng, H. Yu, High-sensitivity infrared attenuated total reflectance sensors for in situ multicomponent detection of volatile organic compounds in water, Nat. Protoc. 11 (2016) 377–386.

[2] D.D. Erbahar, G. Gumus, O. Pamir, E. Musluoglu, V. Ahsen, I. Gurol, M. Harbeck, Polyalkoxy substituted phthalocyanines sensitive to phenolic compounds in water, Sensor. Actuator. B Chem. 227 (2016) 277–282.

[3] L. Mel, J. Feng, L. Wu, J. Zhou, J. Chen, A. Wang, Novel phenol biosensor based on laccase immobilized on reduced graphene oxide supported palladium-copper alloyed nanocages, Biosens. Bioelectron. 74 (2015) 347–352.

[4] F. Vianello, A. Cambria, S. Ragusa, M.T. Cambria, L. Zennaro, A. Rigo, A high sensitivity amperometric biosensor using a monomolecular layer of laccase as biorecognition element, Biosens. Bioelectron. 20 (2004) 315–321.

[5] Q. Zhou, Y. Gao, G. Xie, Determination of bisphenol A, 4-n-nonylphenol, and 4-tert-octylphenol by temperature-controlled ionic liquid dispersive liquid-phase microextraction combined with high performance liquid chromatography-fluorescence detector, Talanta 85 (2011) 1598–1602.

[6] H. Li, J. Yang, M. Gao, J. Wang, B. Sun, Washing rice before cooking has no large effect on the texture of cooked rice, Food Chem. 271 (2019) 388–392.

[7] S.R. Yazdinezhad, A. Ballesteros-Gomez, L. Lunar, S. Rubio, Single-step extraction and cleanup of bisphenol A in soft drinks by hemimicellar magnetic solid phase extraction prior to liquid chromatography/tandem mass spectrometry, Anal. Chim. Acta 778 (2013) 31–37.

[8] J. Lu, J. Wu, P.J. Stoffella, P.C. Wilson, Isotope dilution-gas chromatography/mass spectrometry method for the analysis of alkylphenols, bisphenol A, and estrogens in food crops, J. Chromatogr. A 1258 (2012) 128–135.

[9] X. Wang, X. Lu, L. Wu, J. Chen, 3D metal-organic framework as highly efficient biosensing platform for ultrasensitive and rapid detection of bisphenol A, Biosens. Bioelectron. 65 (2015) 295–301.

[10] S. Yamazaki, S. Itoh, Kinetic evaluation of phenolase activity of tyrosinase using simplified catalytic reaction system, J. Am. Chem. Soc. 125 (2003) 13034–13035.

[11] D. Shan, S. Cosnier, C. Mousty, Layered double hydroxides: an attractive material for electrochemical biosensor design, Anal. Chem. 75 (2003) 3872–3879.

[12] Y. Qu, M. Ma, Z. Wang, G. Zhan, B. Li, X. Wang, H. Fang, H. Zhang, C. Li, Sensitive amperometric biosensor for phenolic compounds based on graphene-silk peptide/tyrosinase composite nanointerface, Biosens. Bioelectron. 44 (2013) 85–88.

[13] N. Yang, X. Chen, T. Ren, P. Zhang, D. Yang, Carbon nanotube based biosensors, Sensor. Actuator. B Chem. 207 (2015) 690–715.

[14] F.R. Caetano, E.A. Carneiro, D. Agustini, L.C.S. Figueiredo-Filho, C.E. Banks, M.F. Bergamini, L.H. Marcolino-Junior, Combination of electrochemical biosensor and textile threads: a microfluidic device for phenol determination in tap water, Biosens. Bioelectron. 99 (2018) 382–388.

[15] H. Furukawa, K.E. Cordova, M. O'Keeffe, O.M. Yaghi, The chemistry and applications of metal-organic frameworks, Science 341 (2013) 974.

[16] F. Li, P. Wang, X. Huang, D.J. Young, H. Wang, P. Braunstein, J. Lang, Large-scale, bottom-up synthesis of binary metal-organic framework nanosheets for efficient water oxidation, Angew. Chem. Int. Ed. 58 (2019) 7051–7056.

[17] H. Li, Y. Wen, X. Zhu, J. Wang, L. Zhang, B. Sun, Novel heterostructure of a MXene@NiFe-LDH nanohybrid with superior peroxidase-like activity for sensitive colorimetric detection of glutathione, ACS Sustain. Chem. Eng. 8 (2020) 520–526.

[18] E. Gkaniatsou, C. Sicard, R. Ricoux, J.-P. Mahy, N. Steunou, C. Serre, Metal-organic frameworks: a novel host platform for enzymatic catalysis and detection, Mater. Horiz. 4 (2017) 55–63.

[19] W. Ma, Q. Jiang, P. Yu, L. Yang, L. Mao, Zeolitic imidazolate framework-based electrochemical biosensor for in vivo electrochemical measurements, Anal. Chem. 85 (2013) 7550–7557.

[20] V. Gascon, E. Castro-Miguel, M. Diaz-Garcia, R.M. Blanco, M. Sanchez-Sanchez, In situ and post-synthesis immobilization of enzymes on nanocrystalline MOF platforms to yield active biocatalysts, J. Chem. Technol. Biotechnol. 92 (2017) 2583–2593.

[21] S. Patra, T.H. Crespo, A. Permyakova, C. Sicard, C. Serre, A. Chausse, N. Steunou, L. Legrand, Design of metal organic framework-enzyme based bioelectrodes as a novel and highly sensitive biosensing platform, J. Mater. Chem. B 3 (2015) 8983–8992.

[22] S. Li, Q. Zhang, Y. Lu, D. Ji, D. Zhang, J. Wu, X. Chen, Q. Liu, One step electrochemical deposition and reduction of graphene oxide on screen printed electrodes for impedance detection of glucose, Sensor. Actuator. B Chem. 244 (2017) 290–298.

[23] S. Cao, D. Yue, X. Li, T.J. Smith, N. Li, M. Zong, H. Wu, Y. Ma, W. Lou, Novel nano-/micro-biocatalyst: soybean epoxide hydrolase immobilized on UiO-66-NH2 MOF for efficient biosynthesis of enantiopure (R)-1, 2-octanediol in deep eutectic solvents, ACS Sustain. Chem. Eng. 4 (2016) 3586–3595.

[24] M. Bilal, M. Adeel, T. Rasheed, H.M.N. Iqbal, Multifunctional metal-organic frameworks-based biocatalytic platforms: recent developments and future prospects, J. Mater. Res. Technol. 8 (2019) 2359–2371.

[25] C. Guo, M. Hu, Z. Li, F. Duan, L. He, Z. Zhang, F. Marchetti, M. Du, Structural hybridization of bimetallic zeolitic imidazolate framework (ZIF) nanosheets and carbon nanofibers for efficiently sensing alpha-synuclein oligomers, Sensor. Actuator. B Chem. 309 (2020) 127821.

[26] M. Wang, M. Hu, Z. Li, L. He, Y. Song, Q. Jia, Z. Zhang, M. Du, Construction of Tb-MOF-on-Fe-MOF conjugate as a novel platform for ultrasensitive detection of carbohydrate antigen 125 and living cancer cells, Biosens. Bioelectron. 142 (2019).

[27] C. Gu, C. Guo, Z. Li, M. Wang, N. Zhou, L. He, Z. Zhang, M. Du, Bimetallic ZrHf-based metal-organic framework embedded with carbon dots: ultra-sensitive platform for early diagnosis of HER2 and HER2-overexpressed living cancer cells, Biosens. Bioelectron. 134 (2019) 8–15.

[28] K. Tian, Y. Ma, Y. Liu, M. Wang, C. Guo, L. He, Y. Song, Z. Zhang, M. Du, Hierarchically structured hollow bimetallic ZnNi MOF microspheres as a sensing platform for adenosine detection, Sensor. Actuator. B Chem. 303 (2020) 127199.

[29] N. Bhardwaj, S.K. Bhardwaj, J. Mehta, K.-H. Kim, A. Deep, MOF-bacteriophage biosensor for highly sensitive and specific detection of staphylococcus aureus, ACS Appl. Mater. Interfaces 9 (2017) 33589–33598.

[30] X. Su, Y. Sun, L. Jin, L. Zhang, Y. Yang, P. Kerns, B. Liu, S. Li, J. He, Hierarchically porous Cu/Zn bimetallic catalysts for highly selective CO2 electroreduction to liquid C-2 products, Appl. Catal. B Environ. 269 (2020) 118800.

[31] J. Xue, Y. Li, J. Hu, Nanoporous bimetallic Zn/Fe-N-C for efficient oxygen reduction in acidic and alkaline media, J. Mater. Chem. 8 (2020) 7145–7157.

[32] Y.F. Li, Z.M. Liu, Y.L. Liu, Y.H. Yang, G.L. Shen, R.Q. Yu, A mediator-free phenol biosensor based on immobilizing tyrosinase to ZnO nanoparticles, Anal. Biochem. 349 (2006) 33–40.

[33] M. Cococcioni, S. de Gironcoli, Linear response approach to the calculation of the effective interaction parameters in the LDA+U method, Phys. Rev. B 71 (2005), 035105.

[34] B.S. Yeo, A.T. Bell, Enhanced activity of gold-supported cobalt oxide for the electrochemical evolution of oxygen, J. Am. Chem. Soc. 133 (2011) 5587–5593.

[35] Y. Wen, C. Ma, Z. Wei, X. Zhu, Z. Li, FeNC/MXene hybrid nanosheet as an efficient electrocatalyst for oxygen reduction reaction, RSC Adv. 9 (2019) 13424–13430.

[36] Y. Wen, T.E. Rufford, X. Chen, N. Li, M. Lyu, L. Dai, L. Wang, Nitrogen-doped Ti3C2Tx MXene electrodes for high-performance supercapacitors, Nano Energy 38 (2017) 368–376.

[37] L. Wu, X. Lu, Dhanjai, Z. Wu, Y. Dong, X. Wang, S. Zheng, J. Chen, 2D transition metal carbide MXene as a robust biosensing platform for enzyme immobilization and ultrasensitive detection of phenol, Biosens. Bioelectron. 107 (2018) 69–75.

[38] J. Feng, G. Zhao, J. Xu, H. Chen, Direct electrochemistry and electrocatalysis of heme proteins immobilized on gold nanoparticles stabilized by chitosan, Anal. Biochem. 342 (2005) 280–286.

[39] Y. Wen, T.E. Rufford, D. Hulicova-Jurcakova, L. Wang, Nitrogen and phosphorous co-doped graphene monolith for supercapacitors, ChemSusChem 9 (5) (2016) 513–520.

[40] Y. Wen, T.E. Rufford, D. Hulicova-Jurcakova, X. Zhu, L. Wang, Structure control of nitrogen-rich graphene nanosheets using hydrothermal treatment and formaldehyde polymerization for supercapacitors, ACS Appl. Mater. Interfaces 8 (2016) 18051–18059.

[41] T. Sagara, K. Niwa, A. Sone, C. Hinnen, K. Niki, Redox reaction mechanism of cytochrome c at modified gold electrodes, Langmuir 6 (1990) 254–262.

[42] N. Zhou, F. Su, C. Guo, L. He, Z. Jia, M. Wang, Q. Jia, Z. Zhang, S. Lu, Two-dimensional oriented growth of Zn-MOF-on-Zr-MOF architecture: a highly sensitive and selective platform for detecting cancer markers, Biosens. Bioelectron. 123 (2019) 51–58.

[43] L. Wu, D. Deng, J. Jin, X. Lu, J. Chen, Nano-graphene-based tyrosinase biosensor for rapid detection of bisphenol A, Biosens. Bioelectron. 35 (2012) 193–199.

[44] F. Wang, C. Yang, C. Duan, D. Xiao, Y. Tang, J. Zhu, An organ-like titanium carbide material (MXene) with multilayer structure encapsulating hemoglobin for a mediator-free biosensor, J. Electrochem. Soc. 162 (1) (2015) B16–B21.

[45] X. Liu, L. Luo, Y. Ding, Y. Xu, Amperometric biosensors based on alumina nanoparticles-chitosan-horseradish peroxidase nanobiocomposites for the determination of phenolic compounds, Analyst 136 (4) (2011) 696–701.

[46] S.Q. Liu, J.H. Yu, H.X. Ju, Renewable phenol biosensor based on a tyrosinase-colloidal gold modified carbon paste electrode, J. Electroanal. Chem. 540 (2003) 61–67.

[47] S. Wang, Y. Tan, D. Zhao, G. Liu, Amperometric tyrosinase biosensor based on Fe_3O_4 nanoparticles-chitosan nanocomposite, Biosens. Bioelectron. 23 (12) (2008) 1781–1787.

[48] L. Lu, L. Zhang, X. Zhang, S. Huan, G. Shen, R. Yu, A novel tyrosinase biosensor based on hydroxyapatite-chitosan nanocomposite for the detection of phenolic compounds, Anal. Chim. Acta 665 (2010) 146–151.

[49] T. Arfin, S.N. Rangari, Graphene oxide-ZnO nanocomposite modified electrode for the detection of phenol, Anal. Methods 10 (2018) 347–358.

[50] J. Ren, T.-F. Kang, R. Xue, C.-N. Ge, S.-Y. Cheng, Biosensor based on a glassy carbon electrode modified with tyrosinase immobilized on multiwalled carbon nanotubes, Microchim. Acta 174 (3-4) (2011) 303–309.

[51] N. Pena, A.J. Reviejo, J.M. Pingarron, Detection of phenolic compounds in flow systems based on tyrosinase-modified reticulated vitreous carbon electrodes, Talanta 55 (2001) 179–187.
[52] M. Portaccio, D. Di Tuoro, F. Arduini, M. Lepore, D.G. Mita, N. Diano, L. Mita, D. Moscone, A thionine-modified carbon paste amperometric biosensor for catechol and bisphenol A determination, Biosens. Bioelectron. 25 (9) (2010) 2003–2008.
[53] Y. Tsai, C. Chiu, Amperometric biosensors based on multiwalled carbon nanotube-Nafion-tyrosinase nanobiocomposites for the determination of phenolic compounds, Sensor. Actuator. B Chem. 125 (2007) 10–16.
[54] G. Darabdhara, B. Sharma, M.R. Das, R. Boukherroub, S. Szunerits, Cu-Ag bimetallic nanoparticles on reduced graphene oxide nanosheets as peroxidase mimic for glucose and ascorbic acid detection, Sensor. Actuator. B Chem. 238 (2017) 842–851.
[55] M. Zhao, Y. Wang, Q. Ma, Y. Huang, X. Zhang, J. Ping, Z. Zhang, Q. Lu, Y. Yu, H. Xu, Y. Zhao, H. Zhang, Ultrathin 2D metal-organic framework nanosheets, Adv. Mater. 27 (2015) 7372.
[56] Y. Wee, S. Park, Y.H. Kwon, Y. Ju, K.-M. Yeon, J. Kim, Tyrosinase-immobilized CNT based biosensor for highly-sensitive detection of phenolic compounds, Biosens. Bioelectron. 132 (2019) 279–285.